Giant Molecular Outflows Powered by Protostars in L1448

Grace A. Wolf-Chase^{1,2}, Mary Barsony^{3,4}, and JoAnn O'Linger⁵

ABSTRACT

We present sensitive ($T_R^* \approx 0.1 K$), large-scale ($47' \times 7'$ -corresponding to 4 pc \times 0.6 pc at the source) maps of the CO J=1 \rightarrow 0 emission of the L1448 dark cloud at 55" resolution. These maps were acquired using the On-The-Fly (OTF) capability of the NRAO 12-meter telescope atop Kitt Peak in Arizona. CO outflow activity is seen in L1448 on parsec-scales for the first time. Careful comparison of the spatial and velocity distribution of our high-velocity CO maps with previously published optical and near-infrared images and spectra has led to the identification of six distinct CO outflows. Three of these are powered by the Class 0 protostars, L1448C, L1448N(A), and L1448N(B). L1448 IRS 2 is the source of two more outflows, one of which is newly identified from our maps. The sixth newly discovered outflow is powered by an as yet unidentified source outside of our map boundaries.

We show the direct link between the heretofore unknown, giant, highly-collimated, protostellar molecular outflows and their previously discovered, distant optical manifestations. The outflows traced by our CO mapping generally reach the projected cloud boundaries. Integrated intensity maps over narrow velocity intervals indicate there is significant overlap of blue- and redshifted gas, suggesting the outflows are highly inclined with respect to the line-of-sight, although the individual outflow position angles are significantly different. The velocity channel maps also show that the outflows dominate the CO line cores as well as the high-velocity wings. The magnitude of the combined flow momenta, as well as the combined kinetic energy of the flows, are sufficient to disperse the 50 M_{\odot} NH₃ cores in which the protostars are currently forming, although some question remains as to the exact processes involved in redirecting the directionality of the outflow momenta to effect the complete dispersal of the parent cloud.

Subject headings: stars: formation—ISM: jets and outflows—methods: observational (On-The-Fly spectral line mapping)—ISM: individual (L1448)—ISM: kinematics and dynamics

1. Introduction

It has long been an open question whether young stars could be the agents of dispersal of their parent molecular clouds through the combined effects of their outflows (Norman & Silk 1979; Bertoldi & McKee 1996). The answer to this question depends on whether the outflows have the requisite kinetic energy to overcome the gravitational binding energy of the cloud, as well as the efficiency with which outflows can transfer momentum, in both magnitude and direction, to the surrounding cloud.

For considerations of molecular cloud dispersal, addressing the question of the adequacy of outflow momenta has historically lagged behind determinations of

outflow energetics. This is because evaluation of the available energy sources needed to account for the observed spectral linewidths in a cloud is adequate for quantitative estimates of outflow energies. However, in order to address whether the requisite momentum for cloud dispersal exists in a given case requires well-sampled, sensitive, large-scale mapping of sufficiently large areas to encompass entire molecular clouds. Such observing capability has been beyond reach until the last few years, with the implementation of "rapid" or "On-The-Fly" mapping capabilities at large-aperture millimeter telescopes.

The fact that many outflows powered by young stellar objects actually extend well beyond their parent molecular cloud boundaries has been recognized only recently, with the advent of large-scale, narrowband optical imaging surveys that have revealed shock-excited Herbig-Haro objects at parsec-scale separations from their exciting sources (Bally, Devine, & Reipurth 1996a; Bally, Devine, & Alten 1996b; Bally et al. 1997; Devine et al. 1997; Eislöffel & Mundt 1997; Wilking et al. 1997; Gomez, Whitney, & Kenyon 1997; Gomez, Whitney, & Wood 1998; Reipurth, Devine, & Bally 1998) and from equally large-area, sensitive, millimeter line maps that

¹Dept. of Astronomy & Astrophysics, University of Chicago, 5640 S. Ellis Ave., Chicago, IL 60637; grace@horta.uchicago.edu

 $^{^2\}mathrm{Adler}$ Planetarium & Astronomy Museum, 1300 S. Lake Shore Drive, Chicago, IL 60605

³NSF POWRE Visiting Professor, Physics Department, Harvey Mudd College, Claremont, CA 91711; barsony@home.com

⁴NSF CAREER Award Recipient

 $^{^5 \}rm Jet$ Propulsion Laboratory, 4800 Oak Grove Dr., MS 100-22, Pasadena, CA 91109; joanno@ipac.caltech.edu

show parsec-scale molecular outflows (Dent, Matthews, & Walther 1995; Lada & Fich 1996; Bence, Richer, & Padman 1996; Bence et al. 1998; O'Linger et al. 1999). The millimeter line maps of parsec-scale flows have been almost exclusively confined to instances of single, well-isolated cases, due to the tremendous confusion of multiple outflows in regions of clustered star formation, such as are found in NGC 1333 (Sandell & Knee 1998; Knee & Sandell 2000), ρ Oph, Serpens (White, Casali, & Eiroa 1995), or Circinus (Bally et al. 1999).

The L1448 dark cloud, with a mass of 100 ${\rm M}_{\odot}$ over its ~ 1.3 pc $\times 0.7$ pc extent as traced by C¹⁸O emission, (Bachiller & Cernicharo 1986a), is part of the much more extensive (10 pc × 33 pc) Perseus molecular cloud complex, which contains $\approx 1.7 \times 10^4 \,\mathrm{M}_{\odot}$, at a distance of 300 pc (Bachiller & Cernicharo 1986b). The two dense ammonia cores within L1448 contain 50 M_{\odot} distributed over a 1 pc \times 0.5 pc area (Bachiller & Cernicharo 1986a; Anglada et al. 1989). The core at V_{LSR} $= 4.2 \text{ km s}^{-1} \text{ contains the Class 0 protostar L1448 IRS 2},$ while the other core, at $V_{LSR} = 4.7 \text{ km s}^{-1}$, harbors four Class 0 protostars: L1448C, L1448N(A), L1448N(B), and L1448NW. (Barsony et al. 1998; O'Linger et al. 1999; Eislöffel 2000). The Class I source, L1448 IRS 1, lies close to the western boundary of the cloud, just outside the lowest NH₃ contours in the maps of (Bachiller & Cernicharo 1986b).

High-velocity molecular gas in L1448 was discovered a decade ago via CO J= $2\rightarrow1$ and CO J= $1\rightarrow0$ mapping of a $\sim 2' \times 6'$ area centered on L1448C, acquired with 12" and 20" angular resolutions, respectively (Bachiller et al. 1990). Due to its brightness, high-velocity extent (\pm 70 km s⁻¹), and symmetrically spaced CO bullets, the L1448C molecular outflow has been the object of much study, unlike the flows from its neighbors, the 7" (in projected separation) protobinary, L1448N(A) & (B), just 1.2' to the north, or L1448 IRS 2, 3.7' to the northwest (e.g., (Curiel et al. 1990; Guilloteau et al. 1992; Bally, Lada, & Lane 1993; Bachiller et al. 1994; Davis et al. 1994; Bachiller et al. 1995; Dutrey, Guilloteau, & Bachiller 1997)). Although outflow activity in the vicinity of the protobinary had been reported previously, the H₂ and CO flows, driven by L1448N(A) and L1448N(B), respectively (Bachiller et al. 1990; Davis & Smith 1995), were not recognized as distinct until recently (Barsony et al. 1998). Identification of these flows was aided by noting the position angle of the lowexcitation H₂ flow, centered on L1448N(A), to be distinct from the position angle of the CO flow from L1448N(B), defined by the direction of the line joining L1448N(B) with the newly discovered Herbig-Haro object, HH 196 (Bally et al. 1997).

Recent, wide-angle ($\sim 70'$ field-of-view), narrowband optical imaging of the entire extent of the L1448 cloud has resulted in the discovery of several systems of Herbig-Haro objects, some displaced several parsecs from any

exciting source (Bally et al. 1997). In order to investigate the link between high-velocity molecular gas and the newly discovered Herbig-Haro objects, as well as to study the possibility of cloud dispersal via outflows, we acquired new, sensitive, large-scale CO J=1 \rightarrow 0 maps of a substantial portion of the L1448 cloud. These new molecular line maps were acquired with the On-The-Fly (OTF) mapping technique as implemented at NRAO's 12-meter millimeter telescope atop Kitt Peak, Arizona.

2. Observations and Data Reduction

The CO J= $1\rightarrow 0$ maps of L1448 presented in this paper were acquired using the spectral-line On-The-Fly (OTF) mapping mode of the NRAO's⁶ 12-meter telescope on 23 June 1997, UT $13^{h}53^{m}$ – UT $19^{h}25^{m}$. We stress that the OTF technique allows the acquisition of large-area, high-sensitivity, spectral line maps with unprecedented speed and pointing accuracy. For comparison, it would have taken eight times the amount of telescope time, or nearly a week in practice, to acquire this same map using conventional, point-by-point mapping. Although OTF mapping is not a new concept, given the rigor of the position encoding that allows precise and accurate gridding of the data, the fast data recording rates that allow rapid scanning without beam smearing, and the analysis tools that are available, the 12-meter implementation is the most ambitious effort at OTF imaging yet.

To produce our CO maps of L1448, we observed a 47′ × 7′ field along a position angle P.A. = 135°, (measured East from North), centered on the coordinates of L1448 IRS 2 ($\alpha_{1950} = 3^h \ 22^m \ 17.9^s$, $\delta_{1950} = 30^\circ \ 34' \ 41''$). The 115 GHz beamwidth was $\approx 55''$. We scanned a total of 33 rows at a rate of 50"/s, along P.A. = 135°, with a row spacing of 12.7". (The row spacing is determined by the optimum spatial sampling and by the scanning position angle.) We calibrated and integrated on an absolute off position ($\alpha_{1950} = 3^h \ 20^m \ 00.0^s$, $\delta_{1950} = 31^\circ \ 00' \ 00''$) at the start of every row. Each row took approximately one minute to scan. Each map coverage took 41 – 56 minutes to complete. We performed six map coverages to attain an RMS in each OTF spectrum of $T_R^* \approx 0.11 \ K$.

A dual-channel, single-sideband SIS receiver was used for all observations. The backend consisted of 250 kHz and 500 kHz resolution filterbanks, yielding velocity resolutions of $0.65~\rm km~s^{-1}$ and $1.3~\rm km~s^{-1}$, respectively. The filterbanks were used in parallel mode, each of the two receiver polarization channels using 256 filterbank channels. The polarization channels were subsequently averaged together to improve signal-to-noise. Only the 250 kHz resolution data were used to produce the maps presented here.

 $^{^6{\}rm The}$ National Radio Astronomy Observatory is a facility of the National Science Foundation, operated under cooperative agreement by Associated Universities, Inc.

Line temperatures at the 12-meter are on the T_R^* scale, and must be divided by the corrected main beam efficiency, η_m^* , to convert to the main-beam brightness temperature scale. For our very extended source, η_m^* is approximately 1.0. Since the corrected main-beam efficiency is the fraction of the forward power in the main diffraction beam relative to the total forward power in the main beam plus error beam, contribution from the error beam can make $\eta_m^* > 1.0$. At 115 GHz, the theoretical error beam width is $\approx 17'$, but the ratio of the error beam amplitude to the main beam amplitude is only 6×10^{-4} , suggesting contribution from the error beam can be ignored. We used the NRAO standard source, B5 $(\alpha_{1950} = 3^h \ 44^m \ 52.4^s, \ \delta_{1950} = 32^\circ \ 44' \ 28'')$, to check absolute line temperatures.

The OTF data were reduced with the Astronomical Image Processing Software (AIPS), Version 15JUL95. AIPS tasks specific to OTF data are 'OTFUV', which converts a single 12-meter OTF map (in UniPOPS SDD format) to UV (single-dish) format, and 'SDGRD', which selects random position single-dish data in AIPS UV format in a specified field of view about a specified position and projects the coordinates onto the specified coordinate system. The data are then convolved onto a grid. OTF data maps were first combined, then gridded into a data cube and baseline-subtracted. Channel maps as well as individual spectra were inspected to ensure good baseline removal and to check for scanning artifacts. Only the first and last rows scanned contained corrupted spectra and were rejected.

3. Results

3.1. The Extent of High-Velocity CO in L1448

Figure 1a shows the extent of high-velocity blue- and redshifted CO J=1→0 emission found within our OTF map boundaries, outlined by the zig-zag lines. The red contours represent high-velocity redshifted emission integrated over the velocity interval 8.1 km s⁻¹ \leq V_{LSR} \leq 17.8 km s⁻¹, whereas the blue contours represent highvelocity blueshifted emission integrated over -12.1 km $\rm s^{-1} \le V_{LSR} \le -1~km~s^{-1}$. The rest velocities of the two NH₃ cores are 4.2 km s⁻¹ and 4.7 km s⁻¹. The mapped area comprises $47' \times 7'$, corresponding to 4 pc \times 0.6 pc at the source, at a distance of 300 pc. Stars indicate the positions of the known Class 0 sources in L1448, which include L1448C, L1448N (the unresolved, 7" separation protobinary L1448N(A) & L1448N(B)), L1448NW (20" northwest of the protobinary), and L1448 IRS 2, at map center. A filled square indicates the position of the Class I Young Stellar Object (YSO), L1448 IRS 1 (Cohen 1980; Eislöffel 2000). Figure 1b, the inset to Figure 1a, shows the scale of the previously mapped region of high-velocity CO, for comparison (from (Bachiller et al. 1990)). This earlier map includes only a small portion of the highvelocity gas associated with Class 0 protostars in L1448.

Comparison of Figures 1a and 1b highlights the truly spectacular spatial extent of outflow activity in L1448.

Figure 2 indicates the positions of all the known Herbig-Haro objects (crosses) which are found within our map boundaries, superimposed on the CO map of Figure 1a. Several striking features are evident in Figure 2: (1) There is a $\sim 15'$ long blueshifted filament that is connected to both the L1448N/L1448C region and to L1448 IRS 2 in a wishbone-shaped structure which contains HH 197, HH 195A-D, HH 196, and culminates in HH 193; (2) There is extended redshifted outflow emission which suggests structure along three separate axes (at P.A.'s \sim 129°, 150°, & 180°) directly to the southeast of L1448N/L1448C; (3) In the immediate vicinity of IRS 2, the blueshifted gas peaks on HH 195E, whereas the center of the red peak is along a line drawn through IRS 2 and HH 195A-D; (4) There is redshifted emission that peaks $\sim 9'$ to the southeast of IRS 2, which lies on a line connecting IRS 2 and HH 193 at P.A.~152°; (5) There is redshifted emission that peaks on HH 277, which appears to be oriented nearly perpendicular to the long axis of our map; (6) There is blueshifted CO emission associated with the HH 267 knots, which lie at the northwestern edge of our map.

In addition to the OTF map, we also acquired single-point spectra of the CO J=1 \rightarrow 0 and ¹³CO J=1 \rightarrow 0 transitions at four positions, as indicated in Figure 3.

These spectra were used to help determine the appropriate velocity integration limits for the high-velocity CO emission shown in Figures 1a and 2. The mapped linewing emission velocities are indicated by the horizontal arrows for the blue-shifted emission in Figures 3a & 3c, and for the red-shifted emission in Figures 3b & 3d. These spectra were also used to determine velocityintervals free of line emission for baseline-subtraction of the gridded OTF data, and to check CO optical depths in the line wings. The spectra shown in Figure 3a were obtained just off the northwest corner of our map, near the HH 267 knots, whereas the spectra of Figures 3b, c, & d were obtained at positions of strong outflow emission within our map boundary. The spectra in Figure 3a show a separate velocity feature at 0 km s⁻¹ in both CO and ¹³CO. The integration limits for the high-velocity gas were chosen conservatively, avoiding emission from the velocity feature at $V_{LSR} = 0 \text{ km s}^{-1}$. It is interesting to note that this velocity feature corresponds to the V_{LSR} of three HH objects in this cloud: HH 196A, HH 196B, & HH 267B.

3.2. Background: Individual Outflow Sources

3.2.1. The L1448C/L1448N Core

The CO outflow from L1448C has been studied extensively since its discovery, at which time it was recognized as a unique source due to its high collimation factor (approaching 10:1) and its extremely high velocities ($\pm 70~{\rm km~s^{-1}}$ – (Bachiller et al. 1990, 1995). Interferometric observations of the outflow, acquired with a 3" × 2.5" synthesized beam, were required to resolve the limb-brightened CO cavities at "low" velocities ($-12 \le V_{LSR} \le +16~{\rm km~s^{-1}}$) (Bachiller et al. 1995; Dutrey, Guilloteau, & Bachiller 1997). By modelling the interferometric CO channel maps, the outflow inclination angle was found to be $i=70^{\circ}$, implying actual jet velocities in excess of 200 km s⁻¹. The initial conical outflow opening half-angle was found to be $\phi/2=22.5^{\circ}$ (Bachiller et al. 1995). The outflow cavity walls become parallel, however, $\approx 1'$ (= 0.08 pc) downstream from the driving source, with a width of $\sim 20''$. Therefore, in our OTF map, the L1448C outflow remains unresolved along its width.

The redshifted lobe of the L1448C outflow is deflected by $\sim 20^{\circ}$ from its initial direction, from an initial position angle of $+160^{\circ}$ to a final position angle of $+180^{\circ}$ (Dutrey, Guilloteau, & Bachiller 1997; Eislöffel 2000). This change in direction of the redshifted flow axis occurs abruptly near the position of the CO "bullet" known as R3 (Bachiller et al. 1990; Dutrey, Guilloteau, & Bachiller 1997). A string of H₂ emission knots along $P.A. = 180^{\circ}$ extends for nearly two arcminutes, beginning about an arcminute southeast of L1448C (Eislöffel 2000). Similarly, the blueshifted CO outflow lobe powered by L1448C starts out at a position angle P.A. = $+159^{\circ}$ (Bachiller et al. 1995), before being deflected through a total angle of $\sim 32^{\circ}$ by the time it arrives an arcminute downstream (Davis & Smith 1995; Eislöffel 2000). This deflection is due to the collision of the blueshifted gas driven by L1448C with the ammonia core containing the protobinary L1448N(A) & (B) (Curiel et al. 1999). The strongly radiative shock emission at this interaction region is evident through various tracers: enhanced CO millimeter line emission at the site of the CO bullet "B3" of Bachiller et al. (1990), a far-infrared continuum emission peak (Barsony et al. 1998), high-excitation, shocked molecular hydrogen emission (Davis et al. 1994; Davis & Smith 1995), and the optically visible shock-excited gas of HH 197 (Bally et al. 1997).

Extrapolating from the vicinity of HH 197 along P.A. $\sim 127^\circ$, which is the axis of the blueshifted L1448C CO outflow after its deflection near HH 197 through knots I, R, and S (Davis & Smith 1995; Eislöffel 2000), leads directly to HH 267. The measured radial velocities of the HH 267 knots (HH 267A: $\rm V_{LSR} = -50~km~s^{-1}$; HH 267B: $\rm V_{LSR} = 0~km~s^{-1}$; HH 267C: $\rm V_{LSR} = -63~km~s^{-1} - Bally$ et al. 1997) and the velocity extent of the blueshifted CO observed by Bachiller et al. (1990) agree well. The reported terminal velocity for the L1448C flow is 70 km s $^{-1}$ (Bachiller et al. 1990, 1995). These two facts led to the suggestion that HH 267 may be powered by L1448C (Barsony et al. 1998).

L1448N(A) and L1448N(B) form a close (7" separation) protobinary (Terebey & Padgett 1997), which is un-

resolved in our OTF map. The redshifted portion of the L1448N(A) flow was first detected via its associated low-excitation molecular hydrogen emission (Davis & Smith 1995). Its exciting source was first correctly identified by Barsony et al. (1998). The corresponding blueshifted lobe has been detected only in an extended, conical reflection nebulosity whose peak is estimated to lie 1."5 west and 6" north of L1448N(A) (Bally et al. 1993). The position angle of $\sim 150^{\circ}$ for this flow is determined by the symmetry axis of the U-shaped shocked molecular hydrogen emission (Barsony et al. 1998; see also Eislöffel 2000) and from the axis of the highly-collimated redshifted CO jet driven by L1448N(A) as seen in the $V_{LSR} = +8 \text{ km s}^{-1}$ outflow channel map of Bachiller et al. (1995).

Redshifted gas associated with the L1448N(B) flow first appears in the paper reporting the discovery of the L1448C outflow (Bachiller et al. 1990). The corresponding blueshifted outflow lobe from L1448N(B) was partially mapped by Bontemps et al. (1996). Barsony et al. (1998) noted that HH 196, a series of blueshifted optical emission knots (HH 196A: $V_{LSR}=0~{\rm km~s^{-1}}$; HH 196B: $V_{LSR}=0~{\rm km~s^{-1}}$; HH 196C: $V_{LSR}=-35~{\rm km~s^{-1}}$; HH 196D: $V_{LSR}=-37~{\rm km~s^{-1}}$ – Bally et al. 1997) lie along the L1448N(B) outflow axis. The position angle of the L1448N(B) outflow is P.A. ~129°.

About 20'' northwest of L1448N(A) lies L1448NW. Recent observations suggest that L1448NW drives a small-scale $\rm H_2$ outflow along an east-west direction (Eislöffel 2000). Although we do not detect a CO outflow associated with L1448NW with our spatial resolution, unpublished interferometric observations do indicate the presence of an E-W flow centered on L1448NW (Terebey 1998).

3.2.2. The L1448 IRS 2 Core

L1448 IRS 2 was confirmed as a Class 0 protostar by O'Linger et al. (1999), who reported a CO outflow associated with this source. The outflow's symmetry axis along P.A. $\sim 133^{\circ}$ and full opening angle, $\phi = 27^{\circ}$, were initially inferred from (1) the locations of HH 195A–D, (2) a fan-shaped reflection nebulosity emanating from IRS 2 in the K' images of Hodapp (1994), (3) the positions of CO "bullets", detected at the 3σ level along the outflow axis about 10' to the northwest of IRS 2, and (4) the apparent V-shaped morphology of the blueshifted CO emission. A more recent, H₂ image of this region has led to a refinement of the IRS 2 outflow axis determination to P.A. $\sim 138^{\circ}$ (Eislöffel 2000).

3.3. Velocity Maps

In order to elucidate the velocity structure of the CO emission, we present Figures 4, 5, & 6. All three figures are presented in rotated coordinates, such that the major axis of our map along P.A. = 135° now lies horizontally.

Figure 4 is meant to be used as a key to identify the HH objects (crosses) and Young Stellar Objects (YSO's-open stars for Class 0 protostars, filled square for the Class I protostar, L1448 IRS1) indicated by the same symbols in the CO veolocity channel maps of Figures 5 & 6. Our beamsize is indicated in the lower right-hand corner of each panel.

Figure 5 shows the contoured greyscale images of the blueshifted integrated CO intensities for five velocity intervals blueward of the ambient cloud velocity, proceeding top down from the highest velocities in the top panel, to the lowest, cloud-core velocities in the bottom panel. Figure 6 shows the same for the redshifted emission. In order to obtain good signal-to-noise, our highest velocity channel maps have been integrated over a 4 km s⁻¹ velocity interval. The other channel maps have been integrated over 2 km s⁻¹ intervals. These maps shed more light on the emission features enumerated in §3.1, and uncover additional information that is not obvious from the outflow map of Figure 2. It is immediately apparent from these maps that much of the emission within the line core delineates gas that has been entrained in the outflows. In particular, the $\sim 15'$ long blueshifted feature, which extends from IRS 2 to HH 193, is seen to some degree in all of the maps depicting emission blueward of the ambient cloud velocity (Figures 5a-e), as well as in the core gas redward of the ambient cloud velocity (Figures 6d & e). Redshifted, as well as blueshifted, CO emission surrounds HH 193. This is not surprising, since the radial velocities and linewidths of HH 193A, B, and C, are -18 & 40 km s⁻¹, 10 & 70 km s⁻¹, and -10 & 50 km s⁻¹, respectively (Bally et al. 1997). This significant overlap of blueshifted and redshifted emission strongly suggests that the blueshifted feature is oriented close to the plane of the sky.

The blueshifted feature is part of a longer feature, which is bipolar about IRS 2 at P.A. $\sim 152^{\circ}$. blueshifted emission is visible as a well-defined structure from $\rm V_{LSR}$ =-8 to 0 km s⁻¹. Similarly, redshifted emission is visible as a well-defined structure from $\rm V_{LSR}$ =8 to 16 km $\rm s^{-1}$. At the highest velocities (Figures 5a & 6a), the blue- and redshifted emission is highly collimated along P.A. $\sim 152^{\circ}$, centered on L1448 IRS 2. However, the blueshifted emission intersects a second blueshifted feature emanating from the L1448N/L1448C region along P.A. $\sim 129^{\circ}$ (Figure 5a). The intersection occurs $\sim 2'$ downstream of the HH 196 knots. A third blueshifted feature branches off to the west $\sim 3'$ downstream from the HH 196 knots (Figure 5b). The redshifted emission along P.A. $\sim 152^{\circ}$ from IRS 2 extends $\sim 9'$ southeast of IRS 2 (Figures 6a-c), where it shows a prominent peak in Figure 6b, as well as in the CO total integrated intensity outflow map in Figure 2.

The blue- and redshifted peaks adjacent to L1448 IRS 2 are most prominent in the lowest-velocity outflow emission (Figures 5c & 6c). The blueshifted peak is spatially

coincident with HH 195E. At higher velocities (Figures 5a & b), the blueshifted emission extends along a P.A. $\sim 125^{\circ}$ from IRS 2, past IRS 1, and may continue past HH 194, which shows a local peak in blueshifted emission (Figures 5b & c). Curiously, the HH 194 knots are all redshifted, with very large linewidths (HH 194A: $V_{LSR}=66~\rm km~s^{-1},~\Delta V{=}110~\rm km~s^{-1};~HH~194B:~V_{LSR}=66~\rm km~s^{-1},~\Delta V{=}150~\rm km~s^{-1};~HH~194C:~V_{LSR}=110~\rm km~s^{-1},~\Delta V{=}60~\rm km~s^{-1}).~HH~194C~has been associated with redshifted outflow emission from IRS 1 (Bally et al. 1997). Although there is a prominent local peak in the blueshifted CO emission at the position of HH~194, there is no evidence of redshifted CO emission (Figures 6a–c) at this position.$

The extended redshifted emission directly to the southeast of L1448N/L1448C is also clearly present at core velocities, very strongly so in Figure 6d, and even in Figure 5e. The previously suggested structure along three separate axes is also seen in Figures 6a–c; mostly strikingly, in Figure 6b. These three axes, along P.A. $\sim 180^{\circ}$, 150° , & 129° , correspond to the PAs of the redshifted lobes of the outflows associated with L1448C, L1448N(A), & L1448N(B), respectively. The redshifted feature that peaks on HH 277 is most prominent as a separate velocity feature in Figure 6c.

In the next section, we consider these features in connection with what is known about the individual outflows in order to interpret the outflow morphology in L1448.

4. DISCUSSION

4.1. Interpretation of Outflow Structure

Figures 7-9 present the various outflow extents and position angles. Figure 7 is relevant for the discussion of alternative interpretations of the outflow emission centered on the L1448 IRS 2 ammonia core. Figure 8 is used for the discussion of the outflows originating from sources embedded in the ammonia core associated with L1448C and L1448N. For both Figures 7 and 8, the outflow axes and extents are superposed on our integrated high-velocity CO linewing map of the L1448 cloud. Figure 9 shows the same outflow axes superposed on a much higher spatial-resolution ($\sim 1''$ vs. $\sim 55''$) H₂ image of the L1448 region from Eislöffel (2000). (This is the only figure using J2000 coordinates.) In all cases (except for the two newly-identified outflow features seen in our CO maps associated with L1448 IRS 2 and the unidentified source outside our map boundaries), outflow position angles were determined from previouslypublished, arcsecond-scale outflow data. For all of the outflows, we find good agreement between large-scale CO features seen in our maps and flow axes that have been determined from the previous, higher-resolution observations. In Figures 7-9, solid, colored lines denote wellestablished flow position angles and extents, derived from our own CO data and the published literature, whereas dashed lines denote outflow position angles and extents that are consistent with our new CO data.

4.1.1. Outflow Emission from the L1448 IRS 2 Ammonia Core

High-velocity CO outflow activity centered on L1448 IRS 2 was discovered from low-spatial resolution ($\approx 55''$) mapping (O'Linger et al. 1999). These authors suggested that L1448 IRS 2 was the source of a single outflow, with a constant opening angle, as depicted in Figure 7a. The previous outflow symmetry axis along P.A. $\sim 133^{\circ}$ and opening angle, $\phi \sim 27^{\circ}$, were derived from the high spatial resolution K' images of Hodapp (1994). We derive a new outflow symmetry axis along P.A. $\sim 138^{\circ}$ from the more recent H₂ images of Eislöffel (2000). Therefore, we have been able to determine more accurately the position angles for the proposed outflow cavity walls, which should lie along P.A. $\sim 152^{\circ}$ and P.A. $\sim 125^{\circ}$, if the IRS 2 outflow retains its initial opening angle out to large distances. This model explains the presence of high-velocity blue- and redshifted CO emission seen along these position angles at large distances from IRS 2, notably the V-shaped morphology of the blueshifted gas and the presence of several CO "bullets" located along the proposed outflow axis, well beyond HH 195A-D. In a constant opening angle outflow scenario, HH 193 lies along one arm of this V, at P.A. $\sim 152^{\circ}$. The blueshifted gas along the other arm of the V (P.A. $\sim 125^{\circ}$) would be confused with emission from the E-W outflow in this vicinity, but since the blueshifted emission extends past IRS 1 towards the redshifted HH 194 knots, at least part of this emission could be due to IRS 2. Although there is redshifted CO emission along P.A. $\sim 138^{\circ}$ and along P.A. $\sim 152^{\circ}$, there is little evidence for redshifted emission along P.A. $\sim 125^{\circ}$. However, this may be due to confusion with the three redshifted lobes associated with L1448C, L1448N(A), & L1448N(B).

Figure 9 clearly shows an outflow associated with IRS 2 along a P.A. $\sim 138^{\circ}$. The redshifted gas along the outflow axis is prominent in the H₂ emission, but is not clearly apparent in our CO maps beyond the redshifted peak about 1' southeast of IRS 2. Hints of more extended emission along P.A. $\sim 138^{\circ}$ may be seen, however, in Figures 6b & c, and curiously, in blueshifted emission extended along this axis to the southeast of IRS 2 in Figure 5d. Such overlap of blueshifted gas along the redshifted outflow axis is expected for outflows oriented nearly in the plane of the sky. Indications of extended blueshifted emission along P.A. $\sim 138^{\circ}$, at least a few arcminutes downstream of HH 195A–D, are seen in Figures 5b & c.

However, there are a few problems with the single outflow, constant opening angle model: (1) Figure 9 indicates that although the initial opening angle of the IRS 2 outflow is $\phi \sim 27^{\circ}$, the two strands of H₂ defining this

opening angle join in a bow shock structure in the vicinity of HH 195A-D; (2) The CO data show little evidence for emission along the cavity wall at P.A. $\sim 125^{\circ}$, although we note that there is much confusion from high-velocity gas associated with other outflows along this position angle to both sides of IRS 2; (3) HH 193 lies precisely at the end of the outflow wall in this model, an unlikely location for a shock; (4) The velocity dispersion of the blueshifted feature along P.A. $\sim 152^{\circ}$ is high, since it is prominent at both ambient cloud velocities and at highly blueshifted velocities (Figures 5, 6d&e); (5) The highest-velocity outflow emission should converge towards the outflow axis (P.A. $\sim 138^{\circ}$) due to projection effects, but the highest-velocity outflow emission lies along P.A. $\sim 152^{\circ}$, the proposed outflow wall.

Our maps are not sensitive enough to have picked up the highest-velocity outflow emission, however, which is severely diluted in our large $(\sim 1')$ beam. Nevertheless, the absence of CO emission along P.A. $\sim 138^{\circ}$ in the highest velocities suggests that the feature along P.A. \sim 152° defines a separate outflow axis. This has led to an alternate interpretation of the high-velocity CO associated with L1448 IRS 2 in which the presence of two outflows is required, as depicted in Figure 7b, with one outflow along P.A. $\sim 138^{\circ}$, and a new, second outflow along P.A. $\sim 152^{\circ}$, so prominent in the CO data. In this scenario, the new IRS 2 outflow would be responsible for exciting HH 193. Two outflows, along distinctly different position angles, would also suggest that IRS 2 is a binary system. Although there is currently no evidence to indicate this source to be binary from available continuum data obtained with the Submillimetre Common User Bolometer Array (SCUBA) at the JCMT on Mauna Kea, Hawaii (O'Linger et al. 1999), it is possible that IRS 2 is a compact binary on a scale smaller than 7" (the resolution of the SCUBA 450 μ m data). Recent work indicates a high incidence of binarity among young stellar systems (eg., Ghez, Neugebauer, & Matthews 1993; Looney, Mundy, & Welch 2000). Only arcsec/sub-arcsec imaging at either millimeter or centimeter wavelengths could test the binary hypothesis further.

Evidence of other outflow activity near L1448 IRS 2 is found by noting that the very confined outflow, whose lobes peak only \sim 1′ on either side of IRS 2, has its redshifted peak well-aligned along the P.A. = 138° outflow that excites HH 195A-D, but the corresponding blue peak closest to IRS 2 is skewed at a somewhat shallower position angle closer to P.A. \sim 125°. No CO emission (Figure 2, Figures 6a-c) is seen along P.A. \sim 125° on the opposite side from IRS 2, which would be expected if there were an outflow along this direction. The blue peak is spatially coincident with HH 195E, however, the only HH 195 knot which is off the P.A. = 138° axis of the IRS 2 outflow. It has been argued that IRS 1 drives an eastwest oriented outflow and is the most probable driving source of HH 195E (Bally et al. 1997; Eislöffel 2000).

Although the presence of such an E-W oriented outflow in this region is undisputed, it is possible that an as yet undiscovered source, other than IRS 1, may be the responsible agent. Thus, the positioning of the blue peak so close to IRS 2 may be coincidental, and due primarily to local heating associated with HH 195 E, and overlapping outflows associated with blueshifted emission from IRS 2 and IRS 1. This picture is supported by the L1448 H₂ mosaic of Eislöffel (2000), shown in Figure 9, which shows the H₂ emission in the vicinity of HH 195E pointing toward IRS 1, not IRS 2.

4.1.2. Outflow Emission from the L1448C/L1448N Ammonia Core

The position angles of the blue- and red-shifted outflowing gas powered by L1448C are indicated by the green lines in both Figures 8 & 9. Solid green lines indicate the L1448C outflow's direction and extent as determined by previous workers (see the caption of Figure 8 for references). The dashed green line on the blue-shifted side represents the continuation of the L1448C outflow proposed by Barsony et al. (1998). The blueshifted L1448C outflow suffers a large deflection from its original direction, as can be seen clearly in Figure 9, which shows the blueshifted L1448C outflow axis passing directly through H₂ emission knots I & S, and about 20" north of emission knot R. Emission knot R lies within more extended H₂ emission that appears to form a Ushaped or bow-shock structure which opens toward the southeast, bisected by the L1448C outflow axis. The sides of the U are separated by $\sim 40''$, with the brighter side (including knot R) lying to the south of the L1448C outflow axis.

This final, deflected, blue-shifted outflow axis lies along P.A. $\sim 127^\circ$, where a long finger of high-velocity blueshifted CO emission is found. Blueshifted CO emission surrounds the HH 267 complex in a horseshoe shape about the proposed extension of the L1448C outflow, suggesting the outflow may be responsible for this emission. The dashed green line on the redshifted side in Figure 8 indicates the possible continuation of the L1448C outflow to the south.

The L1448N(A) molecular outflow axis and extent are depicted by the purple line in Figures 8 & 9. Only redshifted molecular gas associated with the L1448N(A) outflow, along P.A. $\sim 150^\circ$, is detected in our CO maps, with a total length of at least 0.7 pc, as seen in Figure 8. The U-shaped molecular hydrogen emission that traces part of the redshifted outflow cavity wall from the L1448N(A) outflow, as seen in Figure 9, is unresolved in our CO maps. Knots of H₂ emission which trace the outflow wall are $\leq 30''$ apart as far as 3' to the southeast of L1448N(A) (Barsony et al. 1998; Eislöffel 2000). Taken together with the observed length of the CO redshifted lobe, this suggests a collimation factor of at least 16:1. The opening

half-angle of the L1448N(A) outflow was estimated to be $\phi/2 \approx 25^{\circ}$, from the morphology of the near-infrared reflection nebulosity to the north of L1448N(A), associated with what would be the blueshifted outflow lobe (Bally et al. 1993). The blueshifted flow powered by L1448N(A) is not apparent in our CO maps, judging by the drop in the blueshifted, high-velocity CO contour levels along the symmetry axis of its NIR reflection nebula. The lack of blueshifted CO emission from the L1448N(A) outflow is most likely accounted for by the likelihood that the cloud boundary has been reached in this direction, and that the flow has broken out of the molecular cloud.

The L1448N(B) molecular outflow axis and extent are depicted by the mustard-colored lines in Figures 8 & 9. The position angle, P.A. $\sim 129^{\circ}$, of the L1448N(B) outflow was determined by the orientation of the redshifted CO outflow driven by L1448N(B) from Figure 1b and noting that this CO flow symmetry axis intersects HH 196 (Barsony et al. 1998). The true spatial extent of the L1448N(B) CO outflow, however, is demonstrated here for the first time. On the scale of our map, the L1448N(B) outflow remains unresolved along its width. The optical emission knots of HH 196 are, indeed, found to lie right along the L1448N(B) CO outflow axis, confirming the identification of L1448N(B) as their exciting source (Figure 8). Approximately 2' downstream of HH 196, the L1448N(B) flow becomes confused in projection with the P.A. $\sim 152^{\circ}$ outflow from IRS 2. If the outflow continues along P.A. $\sim 129^{\circ}$, it could account for the bulges in the blueshifted emission to the south and southwest of HH 193 (Figure 2, Figure 5c, Figure 8), and might even be responsible for the "C"-shaped blueshifted emission structure east of the HH 267 system, ~ 2.5 parsecs from L1448N(B). The redshifted lobe associated with this source appears to terminate $\sim 2'$ northwest of HH 277, although this could be due to confusion with the highvelocity CO emission surrounding HH 277, which seems to be part of an outflow driven by an unidentified source outside of the boundaries of our map. Using the most conservative length for the L1448N(B) outflow, the major axis taken from the HH 196 knots through the end of the redshifted lobe ($\sim 12'$), the derived lower limit for the collimation factor is >12:1. Estimates of the initial opening angle and width of the L1448N(B) outflow await higher spatial resolution, interferometric imaging.

A dark blue dashed line in Figure 8 indicates a possible outflow axis passing through an otherwise unexplained, high-velocity redshifted feature associated with HH 277, in the southeast quadrant of our CO map. This redshifted CO velocity feature is most prominently seen in Figure 6c. The orientation of this structure is almost perpendicular to the general orientation of our map. Thus, HH 277 is probably driven by a source off the edge of our map.

Finally, although the origin of the HH 267 knots cannot definitively be resolved based on the CO data we present here, our observations do constrain the driving source. L1448N(A) & (B) can be ruled out as possible driving sources of HH 267, since the P.A.'s of their associated outflows are along completely different directions than the lines linking them with HH 267. Furthermore, blue-shifted molecular gas has yet to be detected from L1448N(A). Terminal velocities for the L1448 IRS 2 outflows can not be determined from our data, but the P.A.'s of both of these outflows also miss the HH 267 complex completely. However, the P.A. of the deflected blueshifted lobe of the L1448C flow goes right through HH 267, and the reported terminal velocity for this outflow (70 km s⁻¹: Bachiller et al. 1990, 1995) is in good agreement with the measured HH 267 velocities (Bally et al. 1997), as suggested by Barsony et al. (1998).

4.2. Cloud Dispersal by Giant Protostellar Flows?

The most dramatic evidence for the direct effects of the outflows on the L1448 molecular cloud is seen in the distortions of the cloud contours at all velocities in Figures 5 & 6. Although we cannot estimate the masses and energetics of each individual outflow in our maps due to confusion in space and velocity, we can, nevertheless, estimate the total contribution of the outflows to the cloud's energetics. The Local Thermodynamic Equilibrium (LTE) analysis used to estimate the combined mass of the outflows ($M_{tot} \approx 0.7 M_{\odot}$) is discussed in O'Linger et al. (1999). Optically thin high-velocity CO emission was assumed, given the lack of observed high-velocity ¹³CO emission in the velocity intervals outside the cloud core velocities (see Figure 3). Therefore, the resultant derived mass is a strict lower limit, since no attempt was made to correct for the considerable mass expected to be masked by the line core emission.

For highly inclined outflows $(i > 70^{\circ})$, the characteristic velocity which is used to calculate outflow energetic parameters is best chosen as the geometrical mean between the highest observed velocities, V_{CO} , and the inclination-corrected velocity, $V_{CO}/cos(i-\frac{\phi}{2})$, where $\frac{\phi}{2}$ is the half-opening angle of the outflow (Cabrit & Bertout 1992). Assuming the outflow inclinations, $70^{\circ} \le i \le 90^{\circ}$, $V_{char} = 22 - 34 \text{ km s}^{-1}$ for the L1448 outflows, the total momentum in all the flows is computed to be 16 $\rm M_{\odot}~km~s^{-1} \leq M_{tot} V_{char} \leq 24 \rm \, M_{\odot}~km~s^{-1}$. This range of values is nearly equivalent to the momentum content of the quiescent NH₃ cores, assuming 50 M $_{\odot}$ total cores and $v_{turb} \sim$ 0.5 km s^{-1} (Bachiller & Cernicharo 1986a). Even more striking, the total kinetic energy in all the flows, 2×10^{45} ergs $\leq \frac{1}{2} \mathrm{M}_{tot} \mathrm{V}_{char}^2 \leq 8\times10^{45}$ ergs, exceeds the gravitational binding energy ($\sim GM^2/R \approx 5\times10^{44}$ ergs) of the NH₃ cores by an order of magnitude, and the gravitational binding energy of the 100 M_{\odot} C¹⁸O cloud (9 \times 10⁴⁴ ergs), contained within a 1.3 pc \times 0.7 pc region (Bachiller & Cernicharo 1986b), by a factor of five.

The total outflow momentum quoted above is, in fact, a lower limit, since these outflows are still gaining momentum from the force provided by the central driving engines, and the total outflow mass may be grossly underestimated. The magnitude of both the total energy and momenta of the outflows suggests these outflows are capable of dispersing the NH₃ cores, with the caveat that it is unclear, both from the outflow and ambient cloud morphology, how the outflow momenta can be adequately transferred to the surrounding core. Possibly, this can be accomplished as the individual outflow opening angles increase with time.

5. Summary

- Spectral-line "on-the-fly" mapping was used at the NRAO 12-meter millimeter telescope to produce a large-scale (47′ × 7′) CO (J=1 \rightarrow 0) map of the L1448 dark cloud, sensitive enough (1 σ = 0.1K) to enable the detection of outflow activity on parsec-scales and the identification of six distinct molecular outflows. Large-scale, high-spatial resolution optical and near-infrared images of shocked gas emission regions associated with each outflow were crucial for identifying the CO counterparts of these outflows. Three of the outflows are associated with the Class 0 protostars, L1448N(A), & L1448N(B). Two outflows are associated with the Class 0 protostar, L1448 IRS 2. A sixth outflow, apparently associated with HH 277, is probably driven by an unidentified source located outside of our map.
- For all of the outflows which have previously been identified through high-resolution interferometric observations or small-scale shocked gas emission, we find good agreement between large-scale CO features and flow axes that have been determined from these higher-resolution observations.
- We find evidence of two distinct outflows emanating from the recently-confirmed Class 0 protostar, L1448 IRS 2 (O'Linger et al. 1999), suggesting that IRS 2 is an unresolved binary system. One of these outflows lies along P.A. $\sim 138^{\circ}$, and is apparent both in H₂ emission (Eislöffel 2000) and, to a lesser degree, in our CO data. The second outflow lies along P.A. $\sim 152^{\circ}$ and is seen as a highly-collimated jet in our CO data, culminating, on the blueshifted side, in HH 193.
- The ambient cloud emission contours are severely disturbed by the outflows, suggesting a large fraction of the ambient cloud in the mapped region has been entrained in, or stirred up by, the outflows.
- The total outflow kinetic energy (> 2×10^{45} ergs) and combined outflow momenta (> $16~\rm M_{\odot}~km~s^{-1}$) indicate that the outflows are energetically, and probably dynamically, capable of dispersing the dense ammonia cores out of which the protostellar outflow driving sources of five of the six identified flows, L1448C, L1448N(A), L1448N(B), and L1448 IRS 2, are currently forming.

However, it is unclear, from both the outflow and ambient cloud morphology, how the outflow momenta can be adequately transferred to the surrounding cores.

ACKNOWLEDGEMENTS: We thank Dr. Emerson, Dr. Eric Greisen, and Dr. Jeff Mangum of NRAO for the development, implementation, and improvement of the spectral-line On-The-Fly mapping capability of the 12-meter telescope. GWC, JO, and MB gratefully acknowledge financial support from NSF grant AST-0096087 while part of this work was carried out. Part of this work was performed while GWC held a President's Fellowship from the University of California. MB's NSF POWRE Visiting Professorship at Harvey Mudd College, NSF AST-9731797, provided the necessary time to bring this work to completion. JO acknowledges financial support by the NASA Grant to the Wide-Field Infrared Explorer Project at the Jet Propulsion Laboratory, California Institute of Technology. We would like to thank our referee, John Bally, for his many helpful suggestions which greatly improved this paper.

REFERENCES

- Anglada, G., Rodríguez, L. F., Torrelles, J. M., Estalella, R., Ho, P. T. P., Cantó, J., López, R., & Verdes-Montenegro, L. 1989, ApJ, 31, 208
- Bachiller, R. & Cernicharo, J. 1986a, A&A, 168, 262
- Bachiller, R. & Cernicharo, J. 1986b, A&A, 166, 283
- Bachiller, R., Cernicharo, J., Martin-Pintado, J., Tafalla, M., & Lazareff, B. 1990, A&A, 231, 174
- Bachiller, R., Terebey, S., Jarrett, T., Martin-Pintado, J., Beichman, C.A., & Van Buren, D. 1994, ApJ, 437, 296
- Bachiller, R., Guilloteau, S., Dutrey, A., Planesas, P., & Martin-Pintado, J., 1995, A&A, 299, 857
- Bally, J., Lada, E.A., & Lane, A.P. 1993, ApJ, 418, 322
- Bally, J., Devine, D., & Reipurth, B. 1996a, ApJ, 473, L49
- Bally, J., Devine, D., & Alten, V. 1996b, ApJ, 473, 921
- Bally, J., Devine, D., & Alten, V., & Sutherland, R.S. 1997, ApJ, 478, 603
- Bally, J., Reipurth, B., Lada, C.J., & Billawala, Y. 1999, AJ, 117, 410
- Barsony, M., Ward-Thompson, D., André, P., & O'Linger, J. 1998, ApJ, 509, 733
- Bence, S.J., Richer, J.S., & Padman, R. 1996, MNRAS, 279, 866
- Bence, S.J., Padman, R., Isaak, K.G., Wiedner, M.C., & G.S. Wright 1998, MNRAS, 299, 965
- Bertoldi, F. & McKee, C.F. 1996 in Amazing Light: A Volume Dedicated to C.H. Townes on his 80th Birthday, ed. R.Y. Chiao, New York:Springer
- Bontemps, S., Andr'e, P., Terebey, S., & Cabrit, S. 1996, A&A, 311, 858
- Cabrit, S. & Bertout, C. 1992, A&A, 261, 274
- Cohen, M. 1980, AJ, 85, 29
- Curiel, S., Raymond, J. C., Rodríguez, L. F., Cantó, J. & Moran, J. M. 1990, ApJ, 365, L85
- Curiel, S., Torrelles, J. M., Rodríguez, L. F., Gomez, J. F., & Anglada, G. 1999, ApJ, 527, 310
- Davis, C. J., Dent, W. R. F., Matthews, H. E., Aspin,C., & Lightfoot, J. F. 1994, MNRAS, 266, 933
- Davis, C. J., & Smith, M. D. 1995, ApJ, 443, L41

- Dent, W.R.F., Matthews, H.E., & Walther, D.M. 1995, MNRAS, 277, 193
- Devine, D., Bally, J., Reipurth, B., & Heathcote, S. 1997, AJ, 114, 2095
- Dutrey, A., Guilloteau, S., & Bachiller, S. 1997, A&A, 325, 758
- Eislöffel, J. 2000, A&A, 354, 236
- Eislöffel, J. & R. Mundt 1997, AJ, 114, 280
- Ghez, A.M., Neugebauer, G., & Matthews, K. 1993, AJ, 106, 2005
- Gomez, M., Whitney, B., & Kenyon, S.J. 1997, AJ, 114, 1138
- Gomez, M., Whitney, B., & Wood, K. 1998, AJ, 115, 2018
- Guilloteau, S., Bachiller, R., Fuente, A., & Lucas, R. 1992, A&A, 265, L49
- Hodapp, K.-W. 1994, ApJS, 94, 615
- Knee, L. B. G., & Sandell, G. 2000, to appear in A&A
- Lada, C.J. & Fich, M. 1996, ApJ, 459, 638
- Looney, L.W., Mundy, L.G., & Welch, W.J. 2000, ApJ, 529, 477
- Norman, C. & Silk, J. 1979, ApJ, 234, 86
- O'Linger, J., Wolf-Chase, G.A., Barsony, M., & Ward-Thompson, D. 1999, ApJ, 515, 698
- Reipurth, B., Devine, D., & Bally, J. 1998, AJ, 116, 1396
- Sandell, G., & Knee, L.B.G. 1998, J. R. Astron. Soc. Ca., 92, 32
- Terebey, S. 1998, private communication
- Terebey, S. & Padgett, D. 1997, in IAU Symposium 182, Herbig-Haro Flows and the Birth of Low-Mass Stars, eds. B. Reipurth & C. Bertout (Dordrecht: Kluwer)
- White, G.J., Casali, M.M., & Eiroa, C. 1995, A&A, 298, 594
- Wilking, B.A., Schwartz, R.D., Fanetti, T.M., & Friel, E.D. 1997, PASP, 109, 549

Fig. 1.— High-velocity CO Outflow Emission on Large and Small Scales in the L1448 Dark Cloud

a. Blue contours indicate high-velocity blueshifted $(-12.1 \leq V_{LSR} \leq -1 \text{ km s}^{-1}) \text{ emission and red con-}$ tours indicate high-velocity redshifted (+8.1 $\leq V_{LSR} \leq$ +17.8 km s⁻¹) CO J=1 \rightarrow 0 emission in the 47' \times 7' region we mapped with the NRAO 12-meter telescope. Contour levels start at 2 K km s⁻¹ ($\approx 3 \sigma$), and increase in 1.5 K km s⁻¹ intervals. For comparison, the dashed rectangle shows the approximate area previously mapped (in CO J= $2\rightarrow 1$), shown in the inset. Stars indicate the positions of L1448C, L1448N, L1448NW, and L1448 IRS 2. All of these are Class 0 sources; L1448N is a 7" separation protobinary, consisting of L1448N(A) and L1448N(B). L1448NW lies $\sim 20''$ to the northwest of the protobinary. The filled box indicates the position of the Class I source, L1448 IRS 1. The 55" FWHM NRAO beamsize is indicated in the lower right-hand corner. **b.** The previous CO $J=2\rightarrow 1$ IRAM 30-meter map of highvelocity gas in L1448 (from (Bachiller et al. 1990)): Solid contours indicate high-velocity, blueshifted (-55 km s^{-1} $\leq V_{LSR} \leq 0 \text{ km s}^{-1}$) gas, and dotted contours indicate high-velocity, redshifted (+ 10 km s⁻¹ \leq V_{LSR} \leq + 65 km s⁻¹) gas. First contour and contour intervals are at 10 K km s^{-1} . In addition to the famous protostellar outflow powered by L1448C, the weaker outflow, powered by L1448N(B), is also detected. The 12" FWHM IRAM beamsize is indicated in the lower right-hand corner.

Fig. 2.— CO Outflow Integrated Intensity Map

Names and positions of all the Herbig-Haro objects (black crosses) are shown, as well as the five Class 0 sources (black stars) and the Class I source, L1448 IRS 1 (solid black box). Velocity intervals and contour levels are the same as in Figure 1a.

Fig. 3.— Isotopic CO Spectra

 $^{12}\mathrm{CO}$ (thin solid line) & $^{13}\mathrm{CO}$ (thick solid line) J=1→0 spectra obtained at the four positions on our map whose B1950 coordinates are indicated: (a) CO spectra near the HH 267 knots (just off the northwest corner of our map) clearly show two separate velocity components: a brighter component at the same velocity as HH 267B, V_{LSR} =0 km s⁻¹ (thin vertical dashed line), and a dimmer component at V_{LSR} =4.25 km s⁻¹ (thick vertical dashed line). (b) - (d) CO spectra show strong CO self-absorption at the ambient cloud velocity, V_{LSR} =4.25 km s⁻¹. Arrows indicate the velocity ranges used to determine integrated intensities, masses, and energetics for the outflow emission.

Fig. 4.— Template for Figures 5 & 6

The positions of all the Herbig-Haro objects are indicated by tilted black crosses; the Class I source, L1448 IRS 1, is shown by a filled red box; the Class 0 protostars, L1448 IRS 2, L1448C, L1448N(A) & (B), and

This 2-column preprint was prepared with the AAS IATEX macros v5.0.

L1448NW are indicated by red stars. The separation between L1448C & L1448N is $\sim 80''$.

Fig. 5.— Velocity Channel Maps of Blueshifted Gas

Contoured greyscale images of the integrated CO intensity over velocity intervals blueward of the ambient cloud emission. Velocity intervals, lowest contour levels, and contour intervals, are, respectively: (a) -8 to -4 km s⁻¹, 1 K km s⁻¹, 0.5 K km s⁻¹; (b) -4 to -2 km s⁻¹, 1 K km s⁻¹, 0.5 K km s⁻¹; (c) -2 to 0 km s⁻¹, 1.5 K km s⁻¹, 1 K km s⁻¹; (d) 0 to 2 km s⁻¹, 2 K km s⁻¹, 2 K km s⁻¹; and (e) 2 to 4 km s⁻¹, 2 K km s⁻¹, 2 K km s⁻¹. Positions of Herbig-Haro objects (tilted yellow crosses), IRS 1 (filled red box), and Class 0 objects (red stars) are indicated.

Fig. 6.— Velocity Channel Maps of Redshifted Gas

Contoured greyscale images of the integrated CO intensity over velocity intervals redward of the ambient cloud emission. Velocity intervals, lowest contour levels, and contour intervals, are, respectively: (a) 12 to 16 km s $^{-1}$, 1 K km s $^{-1}$, 1 K km s $^{-1}$; (b) 10 to 12 km s $^{-1}$, 1 K km s $^{-1}$, 1 K km s $^{-1}$; (c) 8 to 10 km s $^{-1}$, 2 K km s $^{-1}$, 1 K km s $^{-1}$; (d) 6 to 8 km s $^{-1}$, 2 K km s $^{-1}$, 2 K km s $^{-1}$; and (e) 4 to 6 km s $^{-1}$, 2 K km s $^{-1}$, 2 K km s $^{-1}$. Positions of Herbig-Haro objects (tilted yellow crosses), IRS 1 (filled red box), and Class 0 objects (red stars) are indicated.

Fig. 7.— Alternate Models for the CO Outflow Emission from L1448 IRS 2

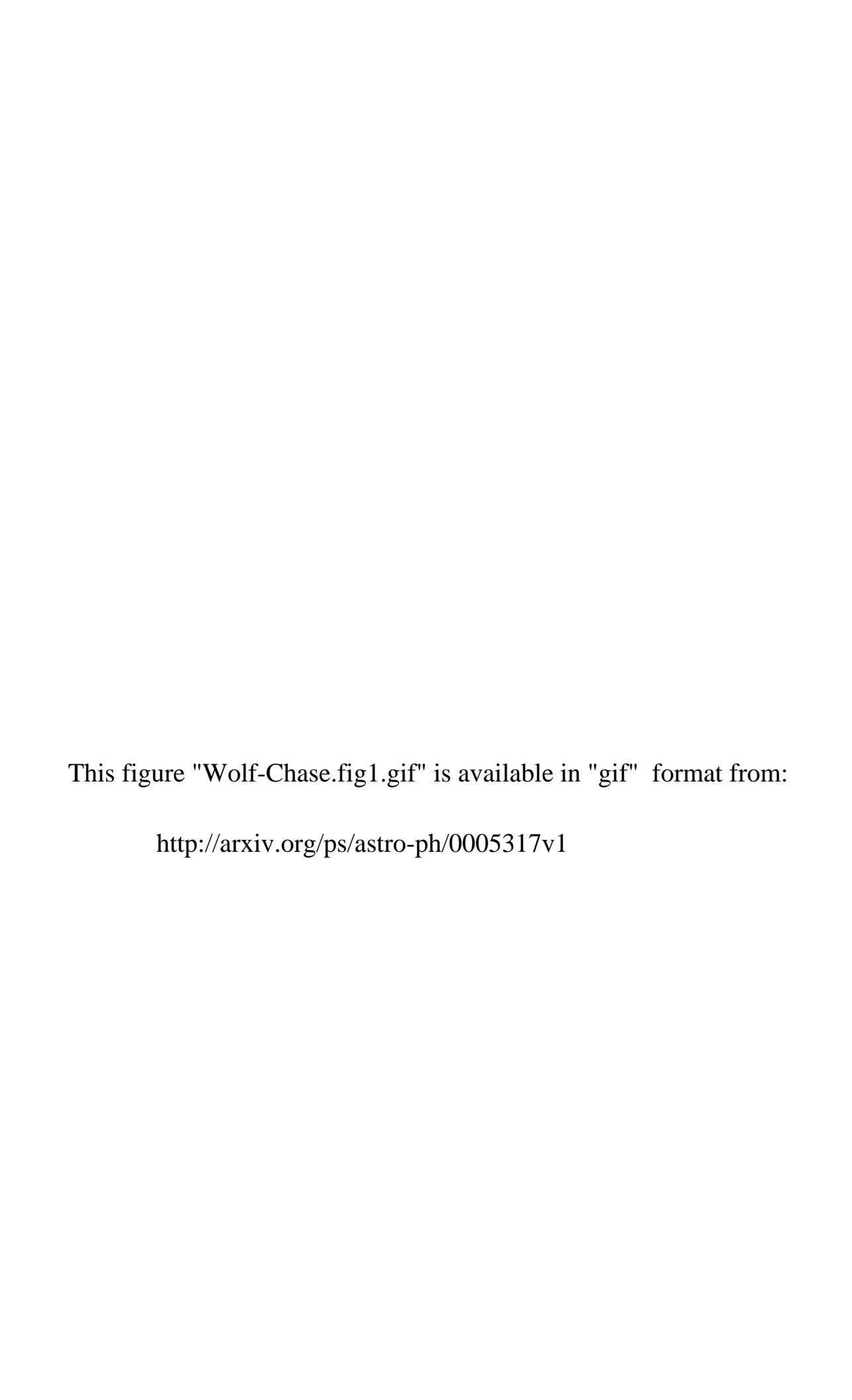
a. One outflow constant-opening angle model (O'Linger et al. 1999). The outflow axis (P.A. $\sim 138^{\circ}$) and corresponding extent of the H₂ emission are denoted by the solid black line. The dashed black line indicates possible extension of this outflow and is based on observed CO bullets along this axis. The dotted lines indicate the outflow walls, determined from a fan-shaped reflection nebulosity ($\phi \sim 27^{\circ}$) seen in K' emission (Hodapp 1994), as well as two strands of H₂ emission originating from IRS 2 which lie along these axes (Eislöffel 2000). b. Two outflows model. Solid and dashed black lines as in Figure 6a. The dashed orange line indicates the axis of the highly-collimated bipolar CO emission which is evident in our CO data. Positions of all the Herbig-Haro objects (black crosses) are shown, as well as the five Class 0 sources (black stars) and the Class I source, IRS 1 (solid black box).

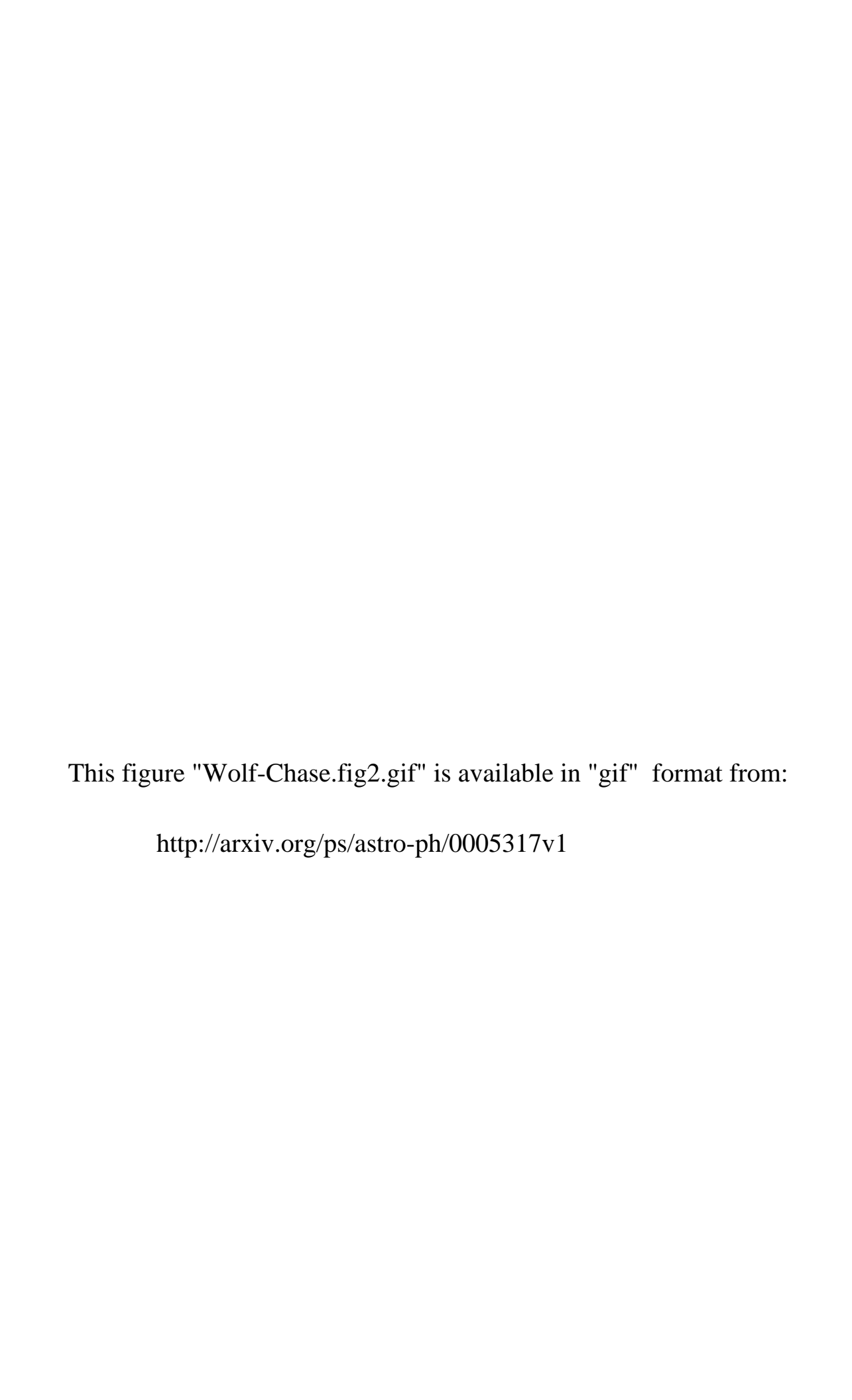
Fig. 8.— Outflow Axes and Extents Superimposed on CO Map

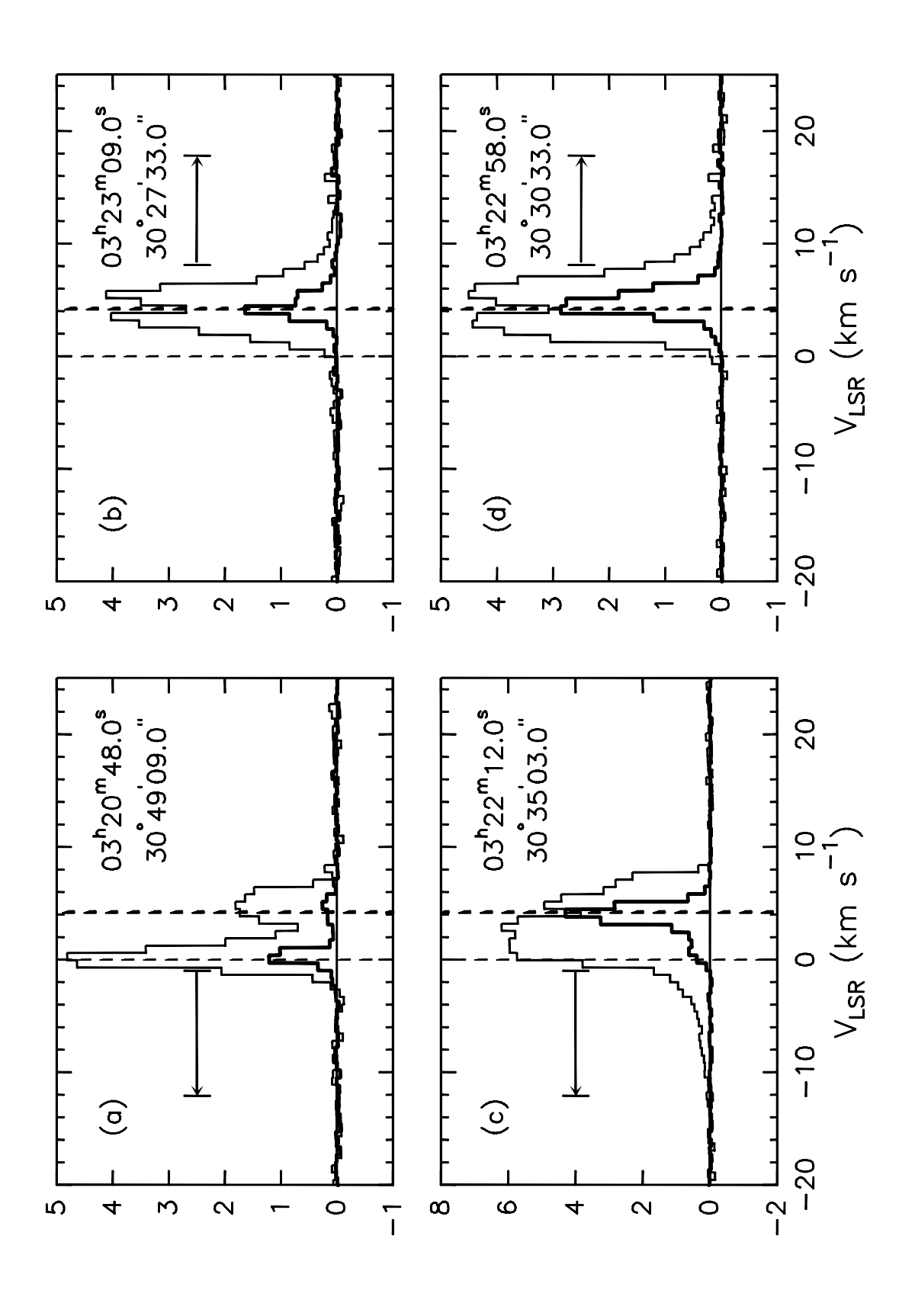
Individual outflow position angles and extents superimposed on the CO outflow integrated intensity map. Positions of all the Herbig-Haro objects (black crosses) are shown, as well as the five Class 0 sources (black stars) and the Class I source, IRS 1 (solid black box). Position angles are indicated for the outflows associated with L1448C (green — Bachiller et al. 1995; Davis & Smith 1995; Dutrey et al. 1997; Eislöffel 2000), L1448N(B) (mustard — Bachiller et al. 1990; Bontemps et al. 1996; Barsony et al. 1998), L1448N(A) (purple — Davis & Smith 1995; Barsony et al. 1998), L1448 IRS 2 (black — O'Linger et al. 1999; orange — this work), and high velocity gas of unknown origin associated with HH 277 (dark blue). The extents of the outflow lobes that are well-established from the literature and our data are indicated with solid lines. Features that are seen only in our CO data, and extrapolations that are consistent with our data, are shown with dashed lines.

Fig. 9.— Outflow Axes and Extents Superimposed on H_2 Map

Individual outflow position angles superimposed on an $\rm H_2$ mosaic of L1448 (Eislöffel 2000). Note that the axes of this figure are in J2000 coordinates. The positions of Herbig-Haro objects (orange crosses), Class 0 sources (red stars), and IRS 1 (open red box), are indicated. Position angles of outflows are indicated as in Figure 8. Note that after its bend at emission knot I, the position angle of the L1448C outflow passes directly through emission knot S. Although emission knot R lies about 20" south of the L1448C outflow axis, this knot appears to be part of extended emission that forms a U-shaped structure which opens toward the southeast, bisected by the outflow axis. The sides of the U are separated by \sim 40", with the brighter side (including knot R) lying to the south of the L1448C outflow axis.







 $T_{\mathsf{R}}^{*}(\mathsf{K})$

 $T_{\mathsf{R}}^{*}(\mathsf{K})$

